scientific reports

OPEN

Alloying effect on the order–disorder transformation in tetragonal FeNi

Li-Yun Tian[1,2✉], Oliver Gutfleisch[3], Olle Eriksson[2,4] & Levente Vitos[1,2,5✉]

Tetragonal (L1$_0$) FeNi is a promising material for high-performance rare-earth-free permanent magnets. Pure tetragonal FeNi is very difficult to synthesize due to its low chemical order–disorder transition temperature (≈ 593 K), and thus one must consider alternative non-equilibrium processing routes and alloy design strategies that make the formation of tetragonal FeNi feasible. In this paper, we investigate by density functional theory as implemented in the exact muffin-tin orbitals method whether alloying FeNi with a suitable element can have a positive impact on the phase formation and ordering properties while largely maintaining its attractive intrinsic magnetic properties. We find that small amount of non-magnetic (Al and Ti) or magnetic (Cr and Co) elements increase the order–disorder transition temperature. Adding Mo to the Co-doped system further enhances the ordering temperature while the Curie temperature is decreased only by a few degrees. Our results show that alloying is a viable route to stabilizing the ordered tetragonal phase of FeNi.

The introduction of neodymium magnets in 1984 was a great leap in magnetic materials[1] and open up many new applications in industry[2]. They are the strongest class of permanent magnets currently available commercially. The downside of this type of magnets, however, is that they include costly rare-earth elements[3–6], that also have the troubling aspect of being difficult to mine without large environmental imprint. Because of these issues, there is strong research interest to develop highly performant permanent magnets that would not depend on the expensive rare-earth elements[7–9]. One of the promising candidates that has emerged is tetragonal L1$_0$ FeNi (tetrataenite), which is known to have large uniaxial magnetic anisotropy, $K_u = 7.0 \times 10^5$ J/m^3[10], and high Curie temperature (T$_c \geq$ 823 K)[11]. While these properties are excellent, the problem is that they are unique for the chemically ordered phase of FeNi and currently there is no efficient way to manufacture the ordered phase due to the low chemical order–disorder transition temperature, T$_{od} \approx$ 593 K[12]. This temperature is simply too low to allow fast enough growth of the ordered phase. Different experimental and theoretical solutions to overcome the problem, such as nitrogen insertion[13,14], are being investigated.

In our previous paper[15] we showed that density functional theory (DFT) as implemented in the Exact Muffin-Tin Orbitals (EMTO) method[16–18] gives an accurate theoretical description of tetragonal FeNi alloys. Our theoretical method predicted the chemical order–disorder transition temperature to be 559 K, which differs from the experimentally value by 34 K (6%) only. The method is a theoretical platform that allows to study how the desirable ordered phase of FeNi can be stabilized at elevated temperatures, which would allow the ordered FeNi phase to be grown in a reasonable amount of time. In the present investigation, we consider the effect of alloying on the properties of tetragonal FeNi. It is our expectation that alloying helps to solve the problems with succesfully synthesizing functional FeNi permanent magnets. Our selection of alloying elements include Al, Ti, Cr, Co, and Mo as representative simple metal, non-magnetic and magnetic 3d metals and a refractory metal, respectively. We study how alloying affects the lattice constants, magnetic moments, Curie temperature, and order–disorder transition temperature. We find that the order–disorder temperature can be increased by suitable choice of the alloying elements and doping concentrations. We therefore predict that selective alloying is a potential way to make synthesizing high-performance magnetic FeNi phase more achievable.

[1]Applied Materials Physics, Department of Materials Science and Engineering, Royal Institute of Technology, 100 44 Stockholm, Sweden. [2]Division of Materials Theory, Department of Physics and Astronomy, Uppsala University, Box 516, 751 20 Uppsala, Sweden. [3]Institute of Materials Science, Technische Universität Darmstadt, 64287 Darmstadt, Germany. [4]School of Science and Engineering, Örebro University, Örebro, Sweden. [5]Research Institute for Solid State Physics and Optics, Wigner Research Center for Physics, Budapest 1525, Hungary. ✉email: liyunt@kth.se; levente@kth.se
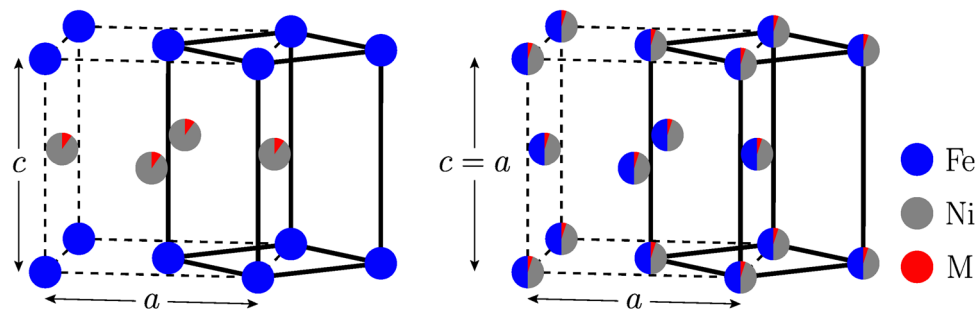
Figure 1. Left panel shows the alloyed L1$_0$ FeNi$_{1-x}M_x$ (M = Al, Ti, Cr, Co, Mo) structure ($\eta = 1$) and the right panel shows the fully random (fcc) structure ($\eta = 0$). Blue atoms are Fe and gray atoms Ni. The letter M and the red part of the atomic sphere indicate the alloying element and its concentration. The convention for the a and c lattice parameters is shown.

Results

In order to keep the magnetic performance of tetragonal FeNi, only small amounts of M substitutions on the Fe/Ni site are adopted. Namely, we consider Fe$_{1-x}M_x$Ni and FeNi$_{1-x}M_x$ with x = 0.05, 0.10 and M = Al, Ti, Cr, Co as well as Fe$_{0.98}$Mo$_{0.02}$Ni, FeNi$_{0.98}$Mo$_{0.02}$, Fe$_{0.93}$Co$_{0.05}$Mo$_{0.02}$Ni and Fe$_{0.95}$Co$_{0.05}$Ni$_{0.98}$Mo$_{0.02}$. The structures of tetragonal M-doped FeNi are treated as Fe$_{1-x}M_x$Ni and FeNi$_{1-x}M_x$ meaning that either the Fe or the Ni layer is doped in the ordered L1$_0$ phase. The disordered sites are described with the coherent potential approximation (CPA)[19,20]. The tetragonal L1$_0$ and the fully disordered structures of FeNi$_{1-x}M_x$ are illustrated in Fig. 1. The left panel shows the substitutional M doping of the Ni layer in the L1$_0$ structure, and the right panel shows the chemically disordered face centered cubic (fcc) structure with homogeneous occupation by the three components. The degree of Fe–Ni disorder is measured by the so-called long-range order parameter η[15], which has values between 0 and 1, corresponding to the fully random and ordered structures, respectively. Ordering effects on the M-doped sublattice in the L1$_0$ phase are not considered, that is we consider the situation when M randomly occupies either the Fe or the Ni sublattice.

The volumes per atom of Fe$_{1-x}M_x$Ni and FeNi$_{1-x}M_x$ (x = 0.05, 0.10) (M = Al, Ti, Cr, Co), as well as Fe$_{0.98}$Mo$_{0.02}$Ni, FeNi$_{0.98}$Mo$_{0.02}$, Fe$_{0.93}$Co$_{0.05}$Mo$_{0.02}$Ni and Fe$_{0.95}$Co$_{0.05}$Ni$_{0.98}$Mo$_{0.02}$ as a function of long-range order parameter η are shown in Fig. 2. The dashed lines refer to the equilibrium volume of undoped FeNi. The volumes of the M-doped FeNi generally decrease slightly as a function of η, which means that the equilibrium volume of the ordered phase ($\eta = 1$) is always smaller than that of the random phase. Results for the tetragonal lattice parameters of the ordered L1$_0$ Fe$_{1-x}M_x$Ni, FeNi$_{1-x}M_x$, Fe$_{0.98}$Mo$_{0.02}$Ni, FeNi$_{0.98}$Mo$_{0.02}$, Fe$_{0.93}$Co$_{0.05}$Mo$_{0.02}$Ni and Fe$_{0.95}$Co$_{0.05}$Ni$_{0.98}$Mo$_{0.02}$, as well as the volume changes relative to L1$_0$ FeNi are listed in Table 1.

From Fig. 2 and Table 1, we can see that only two alloy systems have smaller equilibrium volumes than pure FeNi in the ordered phase: Fe$_{1-x}$Cr$_x$Ni and Fe$_{1-x}$Co$_x$Ni. Furthermore, we observe that Fe substitution leads to smaller equilibrium volumes compared to Ni substitution. This is due to the stronger decrease of the total magnetic moment when Fe is replaced by a dopant compared to FeNi$_{1-x}M_x$. More Fe means larger total magnetic moment, and systems with large magnetic moments tend to have large equilibrium volumes due to the magnetic pressure. In addition, we find that Al, Ti, and Mo increase the volume, which is consistent with the large atomic radii of Al, Ti, and Mo as compared to those of Fe and Ni. The volume increase is the largest for the FeNi$_{1-x}$Ti$_x$ alloys, which is consistent with the above observation. The large volumes of the FeNi$_{1-x}$Ti$_x$ alloys are accompanied by large c/a ratios. Compared to the undoped FeNi alloy, Cr increases the volumes when doping the Ni layer and decreases them when doping the Fe layer. This doping induced reduction of the volume happens because the atomic radii of Cr and Co are not as big as those of Al and Ti and the decreasing Fe content lowers the total magnetic moment, which in turn decreases the equilibrium volume. Cobalt addition negligibly affects the volume when doping on the Ni layer. There is practically no volume change in Fig. 2 and also changes in the magnetic moments are quite small as Table 2 shows. According to the present data, Co can substitute Ni almost perfectly, which is attributable to the fact that Ni and Co are similar chemically. However, Co decreases the volume of FeNi when doping the Fe site.

Total and atomic spin magnetic moments of M-doped FeNi are shown in Table 2 for the ordered ($\eta = 1$) and fully random ($\eta = 0$) phases. The bottom rows of both tables show the magnetic moments of undoped FeNi for comparison. The total magnetic moments of M-doped FeNi are naturally decreased when Fe is replaced by the dopant. Likewise, there is a slight reduction in the magnetic moments when Ni gets replaced, except when doping with Co. All dopants except Co show antiferromagnetic coupling, although for Al, Ti and Mo the moments of the dopants are very small.

It should be noted that doping with Cr causes bigger reductions in total magnetic moment than the non-magnetic Al, Ti, and Mo dopants. Two factors contribute to this. Firstly, the Cr-doped alloys have smaller equilibrium volumes compared to the Al, Ti, and Mo-doped alloys, which means reduced moment due to the magneto-volume effect. Secondly, as Table 2 shows, Cr favors strong antiferromagnetic coupling, which reduces the total magnetic moment.

In our previous paper, we established the order–disorder transition temperature T$_{od}$ of undoped FeNi to be 559 K[15]. Here our goal is to understand in what way alloying affects this temperature, and we are specifically looking for ways to increase this transition temperature. The present theoretical order–disorder transition temperatures
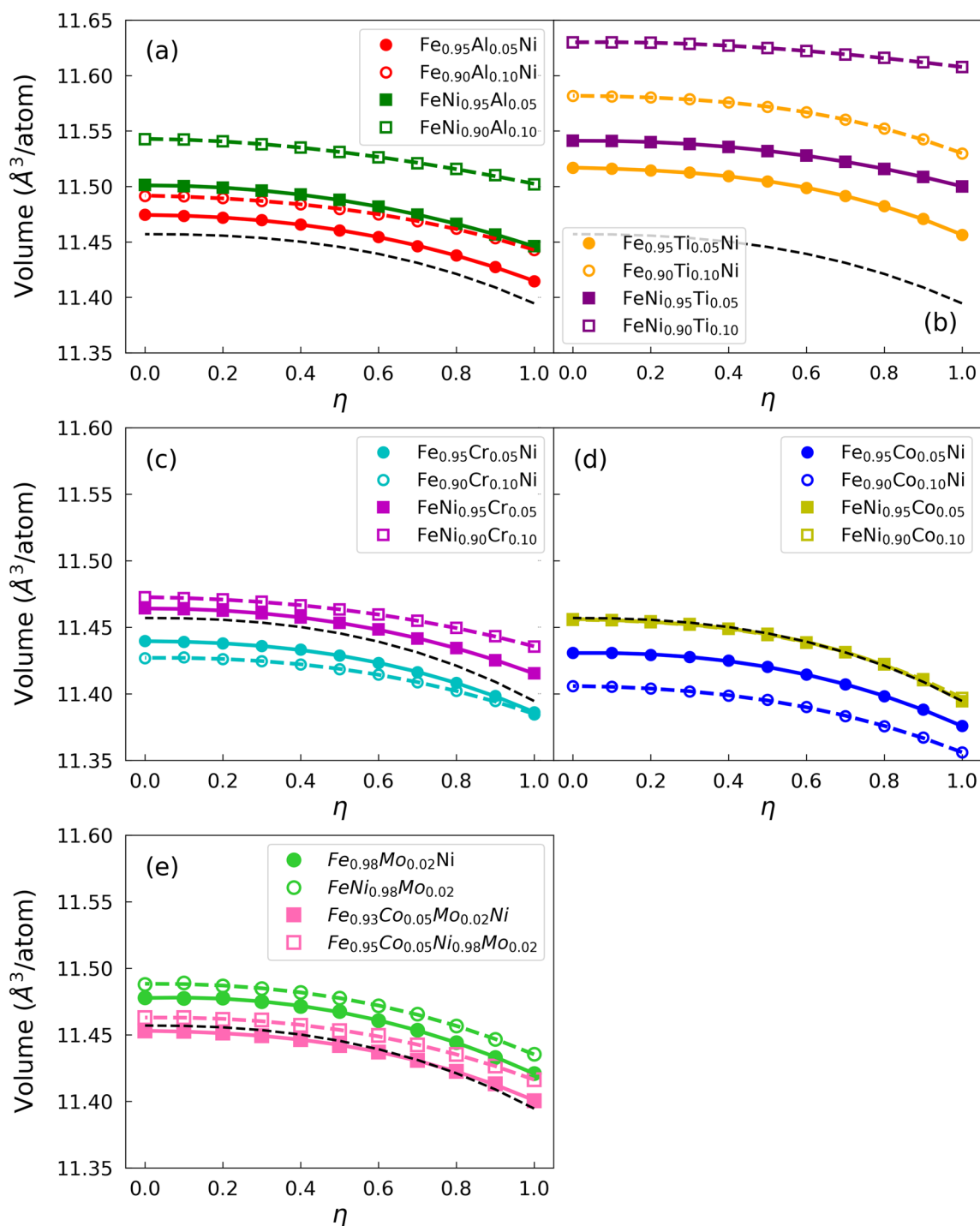
Figure 2. The volume dependence of the long-range order parameter η for the $Fe_{1-x}M_x$Ni and $FeNi_{1-x}M_x$ ($x = 0.05, 0.10$) ($M =$ Al, Ti, Cr, Co), and $Fe_{0.98}Mo_{0.02}$Ni, $FeNi_{0.98}Mo_{0.02}$, $Fe_{0.93}Co_{0.05}Mo_{0.02}$Ni and $Fe_{0.95}Co_{0.05}Ni_{0.98}Mo_{0.02}$ with the EMTO + CPA method. The black dashed line indicates the equilibrium lattice parameter of $L1_0$ FeNi versus the long-range order parameter η.

T_{od} of $Fe_{1-x}M_x$Ni and $FeNi_{1-x}M_x$ alloys, as well as $Fe_{0.98}Mo_{0.02}$Ni, $FeNi_{0.98}Mo_{0.02}$, $Fe_{0.93}Co_{0.05}Mo_{0.02}$Ni and $Fe_{0.95}Co_{0.05}Ni_{0.98}Mo_{0.02}$ are given as a function of dopant concentration M in Fig. 3. The order–disorder transition temperature T_{od} changes differently depending on whether we dope the Fe layer or the Ni layer. A general feature we can identify is that in most cases doping the Fe layer leads to higher transition temperatures compared to doping the Ni layer. Only the Cr case is such where doping the Fe layer decreases the transition temperature compared to Ni layer doping. We ascribe this to the strongly antiferromagnetic nature of Cr.

The changes in the equilibrium volume shows interesting correlation with the transition temperature. For Al, $Fe_{1-x}Al_x$Ni with smaller volume has a larger transition temperature, while $FeNi_{1-x}Al_x$ with bigger volume has a smaller transition temperature. The $FeNi_{1-x}Ti_x$ alloy, which has very large equilibrium volume at high doping

Structures	a	c/a	$\Delta(\%)$	Structures	a	c/a	$\Delta(\%)$
$Fe_{0.95}Al_{0.05}Ni$	3.570	1.004	0.179	$Fe_{0.90}Al_{0.10}Ni$	3.579	0.998	0.424
$Fe_{0.95}Ti_{0.05}Ni$	3.567	1.010	0.544	$Fe_{0.90}Ti_{0.10}Ni$	3.573	1.011	1.188
$Fe_{0.95}Cr_{0.05}Ni$	3.554	1.014	-0.071	$Fe_{0.90}Cr_{0.10}Ni$	3.547	1.021	-0.085
$Fe_{0.95}Co_{0.05}Ni$	3.560	1.008	-0.162	$Fe_{0.90}Co_{0.10}Ni$	3.556	1.010	-0.337
$Fe_{0.98}Mo_{0.02}Ni$	3.563	1.010	0.235	$Fe_{0.93}Co_{0.05}Mo_{0.02}Ni$	3.558	1.012	0.054
$FeNi_{0.95}Al_{0.05}$	3.557	1.017	0.456	$FeNi_{0.90}Al_{0.10}$	3.553	1.026	0.944
$FeNi_{0.95}Ti_{0.05}$	3.564	1.016	0.929	$FeNi_{0.90}Ti_{0.10}$	3.565	1.025	1.872
$FeNi_{0.95}Cr_{0.05}$	3.566	1.007	0.185	$FeNi_{0.90}Cr_{0.10}$	3.568	1.007	0.362
$FeNi_{0.95}Co_{0.05}$	3.570	1.002	0.0005	$FeNi_{0.90}Co_{0.10}$	3.576	0.997	0.022
$FeNi_{0.98}Mo_{0.02}$	3.566	1.009	0.361	$Fe_{0.95}Co_{0.05}Ni_{0.98}Mo_{0.02}$	3.563	1.010	0.193
$FeNi$	3.564	1.007					

Table 1. The lattice parameters (in units of Å) of $Fe_{1-x}M_xNi$ and $FeNi_{1-x}M_x$ ($x = 0.05, 0.10$) ($M =$ Al, Ti, Cr, Co), and $Fe_{0.98}Mo_{0.02}Ni$, $FeNi_{0.98}Mo_{0.02}$, $Fe_{0.93}Co_{0.05}Mo_{0.02}Ni$ and $Fe_{0.95}Co_{0.05}Ni_{0.98}Mo_{0.02}$ as a function of chemical composition for $L1_0$ structures ($\eta = 1$) and the volume changes relative to undoped $L1_0$ FeNi expressed as $\Delta = \frac{V - V_{FeNi}}{V_{FeNi}} \times 100\%$.

	$\eta = 1$					$\eta = 0$				
Structures	m	m_{Fe}	m_{Ni}	m_M		m	m_{Fe}	m_{Ni}	m_M	
$Fe_{0.95}Al_{0.05}Ni$	1.526	1.233	0.296	-0.002		1.503	1.217	0.288	-0.002	
$Fe_{0.90}Al_{0.10}Ni$	1.436	1.157	0.283	-0.004		1.404	1.139	0.270	-0.005	
$Fe_{0.95}Ti_{0.05}Ni$	1.494	1.221	0.286	-0.013		1.471	1.204	0.279	-0.012	
$Fe_{0.90}Ti_{0.10}Ni$	1.375	1.137	0.263	-0.025		1.344	1.115	0.253	-0.024	
$Fe_{0.95}Cr_{0.05}Ni$	1.462	1.227	0.287	-0.052		1.427	1.203	0.279	-0.055	
$Fe_{0.90}Cr_{0.10}Ni$	1.322	1.150	0.269	-0.096		1.262	1.113	0.254	-0.105	
$Fe_{0.95}Co_{0.05}Ni$	1.601	1.248	0.311	0.042		1.577	1.232	0.305	0.040	
$Fe_{0.90}Co_{0.10}Ni$	1.582	1.185	0.312	0.084		1.554	1.169	0.305	0.081	
$Fe_{0.98}Mo_{0.02}Ni$	1.560	1.271	0.295	-0.006		1.536	1.252	0.290	-0.007	
$Fe_{0.93}Co_{0.05}Mo_{0.02}Ni$	1.542	1.210	0.298	0.041	(Co)	1.513	1.190	0.290	0.039	(Co)
				-0.006	(Mo)				-0.007	(Mo)
$FeNi_{0.95}Al_{0.05}$	1.575	1.295	0.283	-0.003		1.548	1.276	0.275	-0.002	
$FeNi_{0.90}Al_{0.10}$	1.534	1.280	0.260	-0.006		1.496	1.255	0.246	-0.005	
$FeNi_{0.95}Ti_{0.05}$	1.544	1.281	0.278	-0.014		1.517	1.263	0.267	-0.013	
$FeNi_{0.90}Ti_{0.10}$	1.472	1.252	0.249	-0.029		1.435	1.229	0.231	-0.025	
$FeNi_{0.95}Cr_{0.05}$	1.499	1.279	0.279	-0.059		1.473	1.262	0.267	-0.055	
$FeNi_{0.90}Cr_{0.10}$	1.385	1.247	0.254	-0.116		1.351	1.226	0.231	-0.106	
$FeNi_{0.95}Co_{0.05}$	1.637	1.308	0.293	0.035		1.626	1.294	0.292	0.040	
$FeNi_{0.90}Co_{0.10}$	1.654	1.305	0.277	0.072		1.645	1.289	0.276	0.080	
$FeNi_{0.98}Mo_{0.02}$	1.578	1.292	0.294	-0.008		1.555	1.276	0.285	-0.007	
$Fe_{0.95}Co_{0.05}Ni_{0.98}Mo_{0.02}$	1.559	1.230	0.296	0.041	(Co)	1.532	1.214	0.285	0.039	(Co)
				-0.008	(Mo)				-0.007	(Mo)
$FeNi$	1.620	1.311	0.309			1.599	1.295	0.304		

Table 2. The total magnetic moments (m) and partial magnetic moments (m_{Fe}, m_{Ni}, m_M) (in unit of μ_B per atom) of $Fe_{1-x}M_xNi$ and $FeNi_{1-x}M_x$ ($x = 0.05, 0.10$) ($M =$ Al, Ti, Cr, Co), and $Fe_{0.98}Mo_{0.02}Ni$, $FeNi_{0.98}Mo_{0.02}$, $Fe_{0.93}Co_{0.05}Mo_{0.02}Ni$ and $Fe_{0.95}Co_{0.05}Ni_{0.98}Mo_{0.02}$ for ordered ($\eta = 1$) and random ($\eta = 0$) phases.

levels, shows rapid decrease of the transition temperature. The $FeNi_{1-x}Co_x$ alloy on the other hand has small equilibrium volumes, but increased transition temperatures.

In all alloy cases, except $FeNi_{1-x}Ti_x$, the maximum T_{od} occurs around $x = 0.05$. We expect the initial increase of T_{od} for small values of x to be caused by the additional configurational entropy created by the dopant. Due to doping the configurational entropy of the ordered state is larger than zero. For small values of x, the proportional entropy gain of the ordered state should be larger than that of the random state. The entropy of the ordered state stabilizes the ordered configuration, as compared to the random state, which leads to the increasing T_{od} for small values of x. Beyond $x = 0.05$, T_{od} starts decreasing, because the DFT total energy difference between ordered and random states starts to decrease significantly, as shown in Fig. 4. By inspection of the DFT energy differences
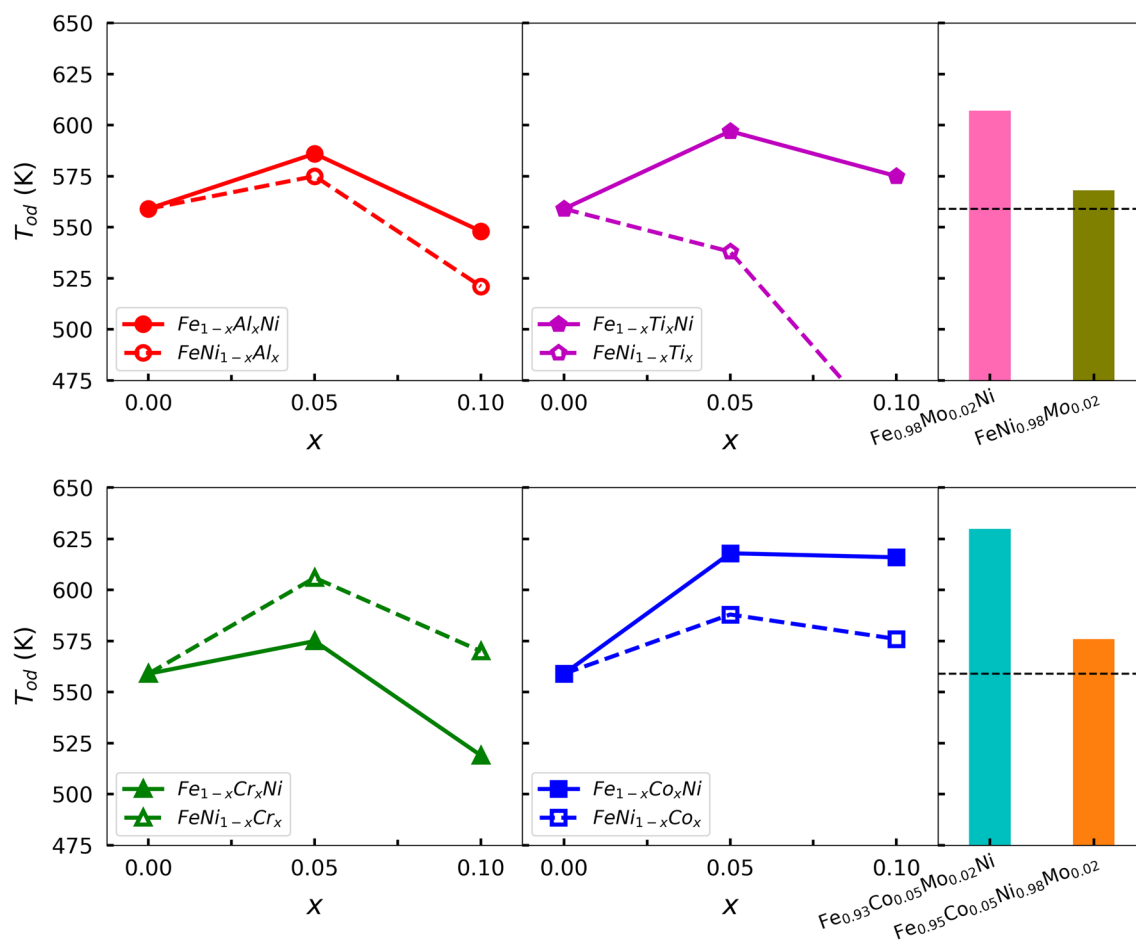
Figure 3. The order–disorder transition temperatures of $Fe_{1-x}M_xNi$ and $FeNi_{1-x}M_x$ ($M =$ Al, Ti, Cr, Co), as well as $Fe_{0.98}Mo_{0.02}Ni$, $FeNi_{0.98}Mo_{0.02}$, $Fe_{0.93}Co_{0.05}Mo_{0.02}Ni$ and $Fe_{0.95}Co_{0.05}Ni_{0.98}Mo_{0.02}$ as a function of the M concentrations. The dashed lines represent the T_{od} (559 K) of $L1_0$ FeNi in the last column.

one can explain why the T_{od} of $Fe_{1-x}Ti_xNi$, $Fe_{1-x}Co_xNi$, and $FeNi_{1-x}Co_x$ alloys does not decrease significantly when going from $x = 0.05$ to $x = 0.10$. Similarly to $Fe_{1-x}Co_xNi$ alloys, $FeNi_{1-x}Cr_x$ have negligible energy differences. In the $FeNi_{1-x}Cr_x$ case, Fig. 3 shows a sizable T_{od} decrease when going from $x = 0.05$ to $x = 0.10$, but this decrease is smaller than that of $Fe_{1-x}Cr_xNi$ alloys, which exhibit significant energy differences.

In Fig. 5, the Curie temperatures T_c are presented for different alloy systems at ordered ($\eta = 1$) and disordered ($\eta = 0$) phases, respectively. All ordered phases have higher T_c than the disordered phases. This predicts that the positive magnetic contribution are likely to increase the order–disorder transition temperature T_{od}. $Fe_{0.90}Co_{0.10}Ni$ alloy has the highest Curie temperatures, which is to say that adding Co into the alloy raises the Curie temperature, which is sensible given the rather high (≈ 1400 K) Curie temperature of pure Co. The Curie temperature of $L1_0$ $Fe_{0.93}Co_{0.05}Mo_{0.02}Ni$ is by only 14.2 K smaller than that of $L1_0$ FeNi.

The highest theoretical order–disorder transition temperatures predicted in the present study are for $Fe_{0.95}Co_{0.05}Ni$ (618 K) and $Fe_{0.93}Co_{0.05}Mo_{0.02}Ni$ (630 K). In both cases, it is assumed that Co and Mo replace Fe within the Fe sublattice. In practice, however, the situation could be more complex. Alloying additions could induce Fe and Ni intermixing or phase decomposition. In the following, we study the energetics of two chemical processes which might prevent the formation of the $L1_0$ phase with Co located on the Fe site in $Fe_{0.95}Co_{0.05}Ni$. In Fig. 6, we consider two different types of scenarios for both Ni-rich and Fe-rich cases. The initial $L1_0$ $Fe_{0.95}Co_{0.05}Ni$ (case A) can change to $Fe_{0.95}Ni_{0.05}$ on the Fe layer and $Ni_{0.95}Co_{0.05}$ on the Ni layer (case B). Alternatively, the initial $L1_0$ $Fe_{0.95}Co_{0.05}Ni$ can separate into pure $L1_0$ FeNi phase plus ferromagnetic fcc NiCo (case C). Similarly, the initial $L1_0$ $FeNi_{0.95}Co_{0.05}$ (case D) can change to $Fe_{0.95}Co_{0.05}$ on the Fe layer and $Ni_{0.95}Fe_{0.05}$ on the Ni layer (case E), or can separate into pure $L1_0$ FeNi phase plus ferromagnetic B2 FeCo (case F). We compute the free energy for each of these processes and check the phase stability as a function of temperature. In this study, the free energies include the configurational and vibrational contributions, but neglect the electronic and magnetic contributions.

First, we discuss the Co doping on the Fe site (cases A, B, and C). According to the free energy differences in Fig. 6, at low temperatures the ordered structure (case A) is more stable than the one with interlayer mixing (case B), but less stable than the phase separated case (case C). At elevated temperatures (above ~ 500 K) these trends are reversed so that the ordered single phase structure is more stable than the phase separation, and the interlayer
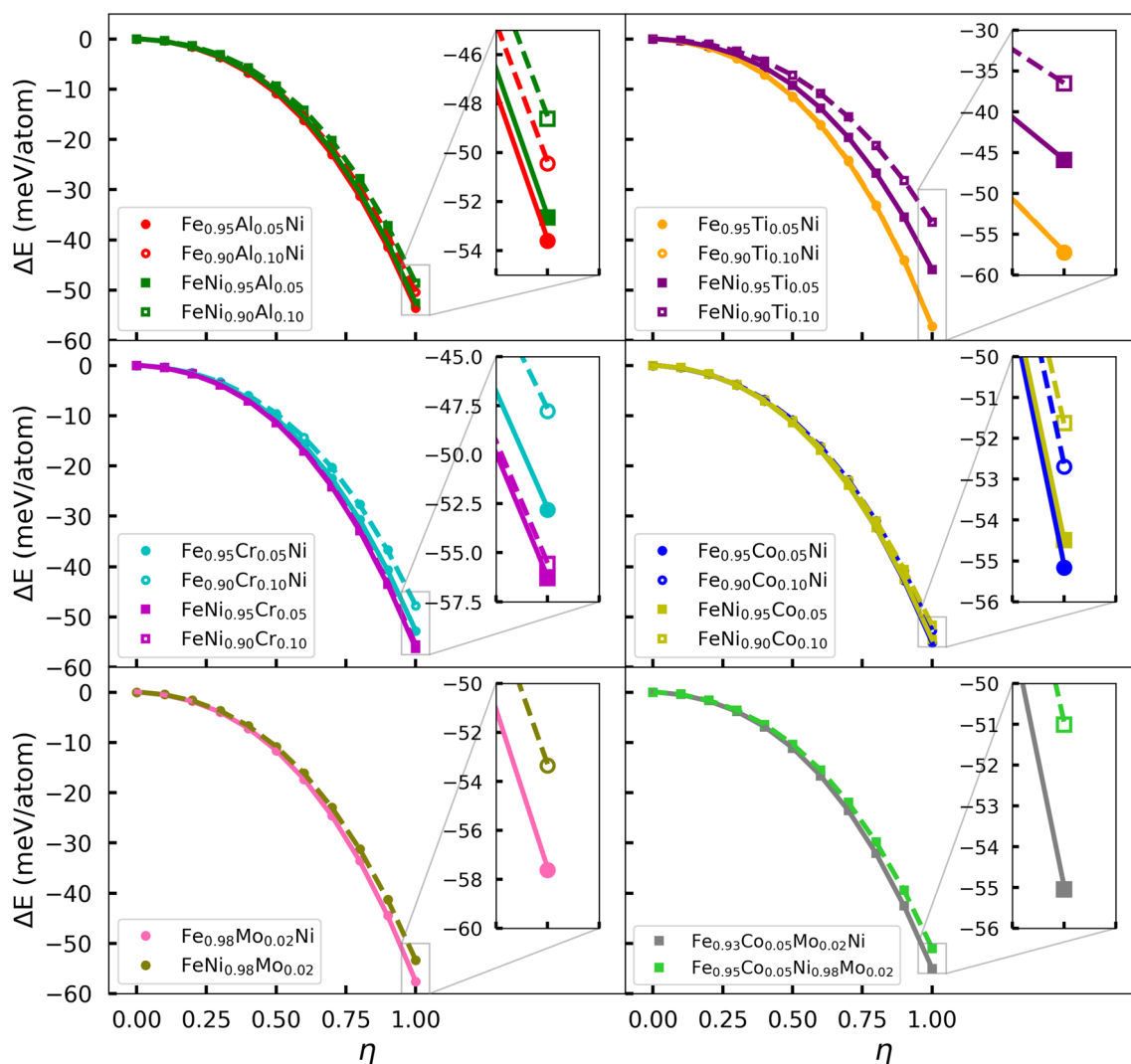
Figure 4. The energies of $Fe_{1-x}M_x$Ni and $FeNi_{1-x}M_x$ (M = Al, Ti, Cr, Co) relative to the energies of fully disordered phases, as well as $Fe_{0.98}Mo_{0.02}$Ni, $FeNi_{0.98}Mo_{0.02}$, $Fe_{0.93}Co_{0.05}Mo_{0.02}$Ni and $Fe_{0.95}Co_{0.05}Ni_{0.98}Mo_{0.02}$ as a function of order parameter.

mixing becomes more stable than the ordered structure. Next, we repeat the Co doping for the Ni site (cases D, E, and F). The overall trends are similar to the doping on the Fe site case. Therefore, the thermodynamic stability seems to prevent the formation of the ideal L1$_0$ $Fe_{0.95}Co_{0.05}$Ni or $FeNi_{0.95}Co_{0.05}$ phases. Considering that phase separation requires substantial diffusion, perhaps its impact is less relevant around the ordering temperature. However, the interlayer mixing, which is mainly driven by the configurational entropy, is predicted to affect the Co partition and thus the largest achievable ordering temperature for the Co-doped FeNi system might be somewhat below the largest values from Fig. 3.

Conclusions

We have studied the effect of alloying on the properties of tetragonal FeNi. Our results show that by alloying it is possible to manipulate the order–disorder transition temperature of FeNi without deteriorating the magnetic properties of the ordered FeNi. We have identified some key insights about how alloying affects the transition temperature. Our results show that the transition temperature increases as a function of dopant concentration up to $x \approx 0.05$. The order–disorder transition temperatures of $Fe_{0.95}Co_{0.05}$Ni and $Fe_{0.93}Co_{0.05}Mo_{0.02}$Ni are 618, 630 K, respectively, which are the highest in the present study. Further alloying causes the transition temperature to decrease. For most dopants studied here substituting Fe leads to a higher transition temperature compared to Ni substitution. At temperatures considered here, Co prefers occupying the Fe site in the Ni-rich L1$_0$ $Fe_{0.95}Co_{0.05}$Ni alloy.
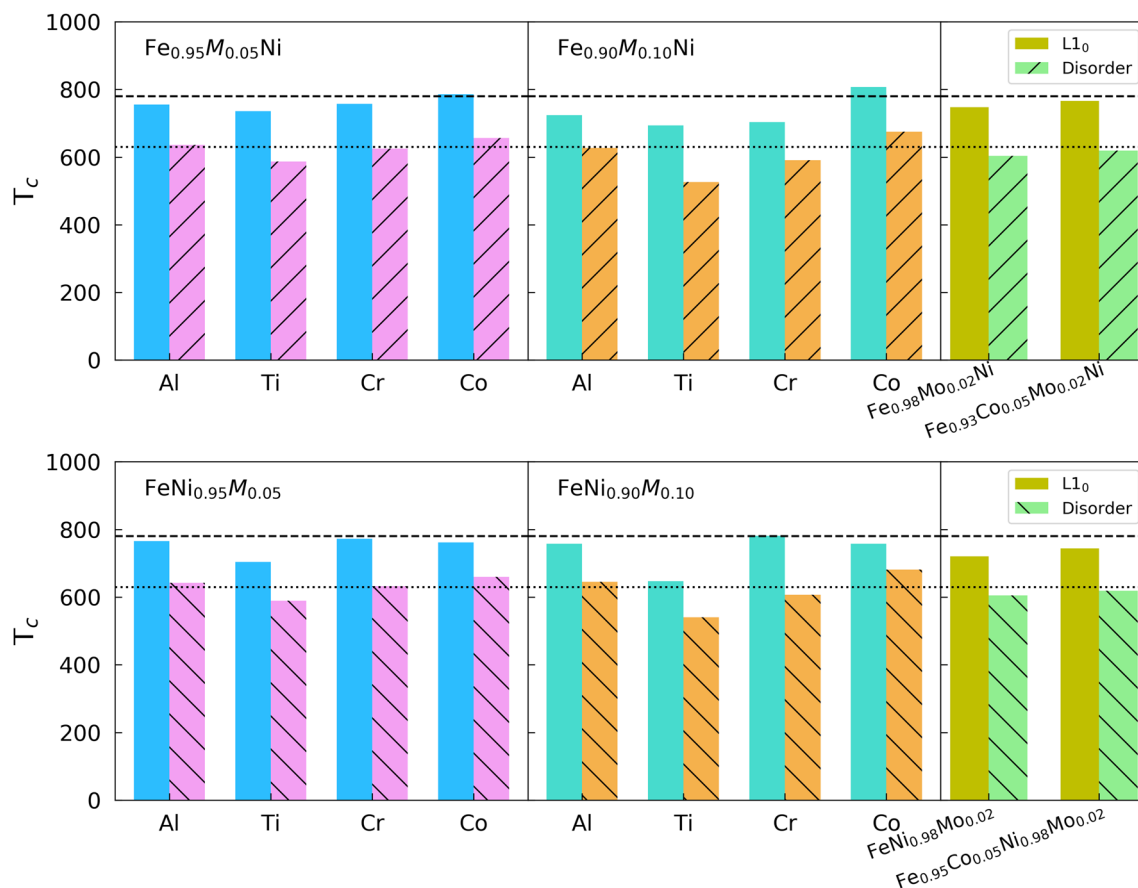
Figure 5. The Curie temperatures of $Fe_{1-x}M_x$Ni and $FeNi_{1-x}M_x$ (M = Al, Ti, Cr, Co), and $Fe_{0.98}Mo_{0.02}$Ni, $FeNi_{0.98}Mo_{0.02}$, $Fe_{0.93}Co_{0.05}Mo_{0.02}$Ni and $Fe_{0.95}Co_{0.05}Ni_{0.98}Mo_{0.02}$ are shown. The dashed lines show the T_c (780 K) of L1$_0$ FeNi, and the dotted lines show the T_c (630 K) of fully random FeNi, respectively.
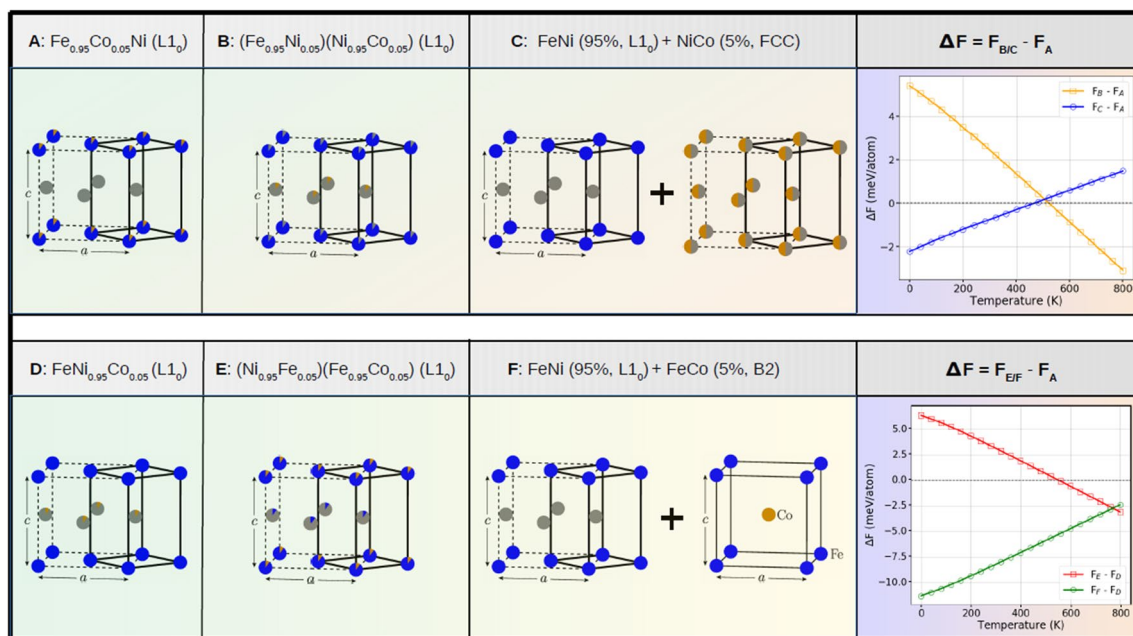

Figure 6. Different types of scenarios which would happen in experiments. Cases *A*, *B* and *C* represent doping on Fe site, and cases *D*, *E* and *F* represent doping on Ni site, respectively. The last column shows the free energy difference between cases *B/C* (*E/F*) and *A* (*D*).

Methods

The first-principles calculations were performed within the exact-muffin-tin orbitals (EMTO) method[16–18] based on Density Functional Theory[21]. The s, p, d, and f orbitals were included in the EMTO basis sets. The single-electron Kohn–Shan equations were solved by the Green's function technique and the compositional disorder was treated using the coherent-potential approximation (CPA)[19,20]. The total energies were computed via the full charge density technique[22]. The exchange-correlation functional was approximated by the Perdew, Burke, and Ernzerhof (PBE)[23] generalized gradient approximation. The magnetic transition temperatures were estimated using the UppASD spin dynamics code[24].

The free energies of ordered, partially ordered and disordered $Fe_{1-x}M_x$Ni and $FeNi_{1-x}M_x$ phases were expressed as a function of η,

$$F(V, T, \eta, x) = E_{0K}(V, \eta, x) - TS_{conf}(\eta, x) + F_{vib}(V, T, \eta, x) + F_{el}(V, T, \eta, x) + F_{mag}(V, T, \eta, x) \quad (1)$$

where E_{0K} is the internal energy per unit cell at 0 K, S_{conf} is the configurational entropy, F_{vib}, F_{el} and F_{mag} are the vibrational, electronic and magnetic free energies, respectively. According to the static Concentration Waves method[25], the configurational entropy of $L1_0$ $Fe_{1-c}(Ni_{1-x}M_x)_c$ (or $(Fe_{1-x}M_x)_{1-c}Ni_c$) were described as a function of LRO parameter η in the form

$$
\begin{aligned}
S_{conf}(\eta, c, x) = \frac{1}{N} \Big[&2 \times c \times (1 + \eta) \times \ln[c \times (1 + \eta)] + 2 \times c \times (1 - \eta) \times \ln[c \times (1 - \eta)] \\
&+ 2 \times (1 - c) \times x \times (1 + \eta) \times \ln[(1 - c) \times x \times (1 + \eta)] \\
&+ 2 \times (1 - c) \times x \times (1 - \eta) \times \ln[(1 - c) \times x \times (1 - \eta)] \\
&+ 2 \times (1 - c) \times (1 - x) \times (1 + \eta) \times \ln[(1 - c) \times (1 - x) \times (1 + \eta)] \\
&+ 2 \times (1 - c) \times (1 - x) \times (1 - \eta) \times \ln[(1 - c) \times (1 - x) \times (1 - \eta)] \Big].
\end{aligned}
\quad (2)
$$

Here the atomic fraction of the solute c equals to 0.5 and x is 0.05 or 0.10. Total atomic number N equals to 4 in $L1_0$ structure. Detailed information about the approach can be found in Ref.[25].

The vibrational contribution to Helmholtz free energy, $F_{vib}(V, T, \eta, x) = E_{vib} - TS_{vib}$, was described by Debye model with the Debye temperatures determined by the tetragonal elastic parameters. The electronic contribution to free energy was estimated by $F_{el} \approx -\frac{1}{2} TS_{el}(V, \eta, x) \approx -\frac{2\pi^2}{3} k_B^2 T^2 N_{el}(\varepsilon_F, \eta, x)$, where electronic density of state $N_{el}(\varepsilon_F, \eta)$ is approximated to be constant in the neighborhood of the Fermi level ϵ_F. The magnetic contribution to free energy, $F_{mag}(V, T, \eta, x) = -TS_{mag}(V, T, \eta, x) = -T \frac{\partial \langle H_{mag}(V,T,\eta,x) \rangle}{\partial T}$, and Heisenberg exchange Hamiltonian $H_{mag}(V, T, \eta, x) = -\frac{1}{2} \sum_{i \neq j} J_{ij} \mu_i \mu_j \hat{e}_i \hat{e}_j$ where J_{ij} is the Heisenberg exchange interaction between atoms i and j, and μ_i and μ_j are the local magnetic moments on sites i and j. The order–disorder temperature T_{od} was then obtained by computing $\partial \eta / \partial T$.

References

1. Sagawa, M., Fujimura, S., Togawa, N., Yamamoto, H. & Matsuura, Y. New material for permanent magnets on a base of Nd and Fe. *J. Appl. Phys.* **55**, 2083–2087 (1984).
2. Gutfleisch, O. *et al.* Magnetic materials and devices for the 21st century: stronger, lighter, and more energy efficient. *Adv. materials* **23**, 821–842 (2011).
3. Lewis, L. H. & Jiménez-Villacorta, F. Perspectives on permanent magnetic materials for energy conversion and power generation. *Metall. Mater. Trans. A* **44**, 2–20 (2013).
4. Lewis, L. H. *et al.* Inspired by nature: investigating tetrataenite for permanent magnet applications. *J. Phys. Condens. Matter* **26**, 064213 (2014).
5. Bordeaux, N., Montes-Arango, A. M., Liu, J., Barmak, K. & Lewis, L. H. Thermodynamic and kinetic parameters of the chemical order-disorder transformation in L10 FeNi (tetrataenite). *Acta Mater.* **103**, 608–615. https://doi.org/10.1016/j.actamat.2015.10.042 (2016).
6. Maât, N. *et al.* Creating, probing and confirming tetragonality in bulk FeNi alloys. *Acta Mater.* **196**, 776–789. https://doi.org/10.1016/j.actamat.2020.07.019 (2020).
7. Skomski, R. *et al.* Predicting the future of permanent-magnet materials. *IEEE Trans. Magn.* **49**, 3215–3220 (2013).
8. Skokov, K. & Gutfleisch, O. Heavy rare earth free, free rare earth and rare earth free magnets-vision and reality. *Scr. Mater.* **154**, 289–294 (2018).
9. Kuz'Min, M., Skokov, K., Jian, H., Radulov, I. & Gutfleisch, O. Towards high-performance permanent magnets without rare earths. *J. Phys. Condens. Matter* **26**, 064205 (2014).
10. Kojima, T. *et al.* Fe–Ni composition dependence of magnetic anisotropy in artificially fabricated L1₀-ordered FeNi films. *J. Phys. Condens. Matter* **26**, 064207 (2014).
11. Wasilewski, P. Magnetic characterization of the new magnetic mineral tetrataenite and its contrast with isochemical taenite. *Phys. Earth Planet. Inter.* **52**, 150–158 (1988).
12. Néel, L., Pauleve, J., Pauthenet, R., Laugier, J. & Dautreppe, D. Magnetic properties of an Iron–Nickel single crystal ordered by neutron bombardment. *J. Appl. Phys.* **35**, 873–876 (1964).
13. Goto, S. *et al.* Synthesis of single-phase L1₀-FeNi magnet powder by nitrogen insertion and topotactic extraction. *Sci. Rep.* **7**, 13216 (2017).
14. Takata, F., Ito, K. & Suemasu, T. Fabrication of ordered Fe–Ni nitride film with equiatomic Fe/Ni ratio. *Jpn. J. Appl. Phys.* **57**, 058004 (2018).

15. Tian, L.-Y. *et al.* Density functional theory description of the order–disorder transformation in Fe–Ni. *Sci. Rep.* https://doi.org/10.1038/s41598-019-44506-7 (2019).
16. Vitos, L., Skriver, H. L., Johansson, B. & Kollár, J. Application of the exact muffin-tin orbitals theory: the spherical cell approximation. *Comput. Mater. Sci.* **18**, 24–38 (2000).
17. Vitos, L., Abrikosov, I. & Johansson, B. Anisotropic lattice distortions in random alloys from first-principles theory. *Phys. Rev. Lett.* **87**, 156401 (2001).
18. Vitos, L. *Computational Quantum Mechanics for Materials Engineers: The EMTO Method and Applications* (Springer, Berlin, 2007).
19. Soven, P. Coherent-potential model of substitutional disordered alloys. *Phys. Rev.* **156**, 809 (1967).
20. Gyorffy, B. Coherent-potential approximation for a nonoverlapping-muffin-tin-potential model of random substitutional alloys. *Phys. Rev. B* **5**, 2382 (1972).
21. Yang, W. & Ayers, P. W. Density-functional theory. In *Computational Medicinal Chemistry for Drug Discovery*, 103–132 (CRC Press, 2003).
22. Vitos, L. Total-energy method based on the exact muffin-tin orbitals theory. *Phys. Rev. B* **64**, 014107 (2001).
23. Perdew, J. P., Burke, K. & Ernzerhof, M. Generalized gradient approximation made simple. *Phys. Rev. Lett.* **77**, 3865 (1996).
24. Skubic, B., Hellsvik, J., Nordström, L. & Eriksson, O. A method for atomistic spin dynamics simulations: implementation and examples. *J. Phys. Condens. Matter* **20**, 315203 (2008).
25. Khachaturyant, A. G. *Theory of Structural Transformations in Solids* Vol. 1983 (Wiley, New York, 1983).

Acknowledgements

Author contributions

L. T. performed the calculations and the research; L. T. analysed the data and wrote the manuscript; L. V. conceived and supervised the work; L. V., O. G. and O. E. initiated this research, discussed the results and commented on the manuscript.

Funding

Competing interests

The authors declare no competing interests.

Additional information

Correspondence and requests for materials should be addressed to L.-Y.T. or L.V.

Reprints and permissions information is available at www.nature.com/reprints.

Publisher's note Springer Nature remains neutral with regard to jurisdictional claims in published maps and institutional affiliations.